Journal of Solid State Chemistry 184 (2011) 1459–1464

Contents lists available at ScienceDirect

Journal of Solid State Chemistry

journal homepage: www.elsevier.com/locate/jssc

# Selective hydrothermal synthesis of BiOBr microflowers and $Bi_2O_3$ shuttles with concave surfaces

Peipei Xiao, Lingling Zhu, Yongchun Zhu *, Yitai Qian *

*Hefei National Laboratory for Physical Science at Microscale and Department of Chemistry, University of Science and Technology of China, Hefei, Anhui 230026, People's Republic of China*

ARTICLE INFO

*Article history:*
Received 6 December 2010
Received in revised form
5 March 2011
Accepted 7 April 2011
Available online 16 April 2011

*Keywords:*
BiOBr
$Bi_2O_3$
Microflowers
Shuttles
Hydrothermal synthesis

ABSTRACT

Through controlling the amount of NaOH added, BiOBr and $Bi_2O_3$ with different shapes were hydrothermally synthesized in the reaction system of $Bi(NO_3)_3$-hexadecyl trimethyl ammonium bromide (CTAB)-NaOH. As 8 mmol of NaOH was added, BiOBr microflowers constructed of nanoflakes were synthesized. The thickness of these single-crystal nanoflakes was about 20 nm. In the similar condition, when the amount of NaOH added was 28 mmol, $Bi_2O_3$ shuttles with concave surfaces were obtained. The length of these shuttles was 100 μm and the diameter at the middle of these shuttles was 50 μm. The photocatalytic activity of as-prepared BiOBr microflowers was evaluated by the degradation of methyl orange (MO) under visible-light irradiation ($\lambda > 420$ nm), which was up to 96% within 90 min.



## 1. Introduction

In the last years, synthesis and characterization of bismuth compounds have received a great attention due to their potential applications. It was reported that BiOBr had a higher photocatalytic performance compared to P25 ($TiO_2$ nanoparticles) under UV illumination [1]. BiOBr nanoplate microspheres were used to remove NO in indoor air under visible light irradiation [2]. $Bi_2O_3$ can be used in microelectronics [3], optical coatings [4], oxide–ion conductors [5], piezo-optic materials [6], solar cells [7], gas sensors [8,9], ceramic glass manufacturing [10] and supercapacitors [11,12].

Hydrothermal/solvothermal methods have been used to prepare BiOBr and $Bi_2O_3$ microstructures/nanostructures. BiOBr micro- and nanosheets were synthesized by the hydrogen peroxide ($H_2O_2$) direct oxidation of bulk metal bismuth (Bi) particles followed by a hydrothermal treatment [13]. BiOBr microspheres were synthesized by employing ethylene glycol as the solvent [14–16]. BiOBr lamellar structures were prepared using CTAB as Br source and the photocatalytic efficiency of the product by the degradation of methyl orange (MO) under visible-light irradiation was up to 96% within 120 min [17]. $Bi_2O_3$ nanoplates were fabricated directly from commercial bulk bismuth oxide crystals by a hydrothermal treatment [18]. $Bi_2O_3$ nanowires were prepared on a protein-assisted hydrothermal route [19].

Herein, we report the hydrothermal synthesis of BiOBr microflowers and $Bi_2O_3$ shuttles with concave surfaces in the reaction system of $Bi(NO_3)_3$–CTAB–NaOH by changing the amount of NaOH. When the amount of NaOH added was 8 mmol, BiOBr microflowers composed of nanoflakes were hydrothermally synthesized. In the similar condition, as 28 mmol of NaOH was added, $Bi_2O_3$ shuttles with concave surfaces were obtained. Furthermore, the photocatalytic activities and the stability of the as-prepared BiOBr samples were also studied.

## 2. Experimental section

### 2.1. Sample preparation

All the reagents were of analytical purity, purchased from Shanghai Chemical Company, and used without the further purification. In a typical synthesis of BiOBr microflowers, $Bi(NO_3)_3 \cdot 5\,H_2O$ (1 mmol) was dissolved in 2 ml of diluted nitric acid (2 mol $L^{-1}$) in a beaker, and 20 ml of CTAB (1.5 mmol) solution was added into the above solution with continuous stirring. After that, 20 ml of NaOH (8 mmol) solution was added into the mixed solution. The final solution was stirred for 30 min and then transferred to a stainless steel Teflon-lined autoclave with the volume of 60 ml. The autoclave was sealed and maintained at 120 °C for 12 h. After the reaction, the autoclave was

* Corresponding authors. Fax: +86 551 360 7402.
*E-mail addresses:* ychzhu@ustc.edu.cn (Y. Zhu), ytqian@ustc.edu.cn (Y. Qian).

0022-4596/$ - see front matter © 2011 Elsevier Inc. All rights reserved.
doi:10.1016/j.jssc.2011.04.015

cooled to room temperature naturally. The product was collected by centrifugation, washed several times with distilled water and absolute ethanol, and dried under vacuum at 60 °C for 6 h.

BiOBr nanoflakes were prepared without adding NaOH while keeping other parameters unchanged.

$Bi_2O_3$ rod clusters or shuttles with concave surfaces were obtained using 13 mmol or 28 mmol of NaOH while keeping other parameters unchanged, respectively.

### 2.2. Sample characterization

The products were characterized by using X-ray power diffraction (XRD) recorded on a Japanese Rigaku D/max-gA rotating anode diffractometer equipped with monochromatic high-intensity Cu $K\alpha$ radiation ($\lambda = 1.54178$ Å). The scanning electron microscopy (SEM) images were taken using a field-emitting scanning electron microscope (FESEM, JEOL–JSM-6700 F). The transmission electron microscopy (TEM) images, SAED pattern, high-resolution transmission electron microscopy (HRTEM) images and an energy-dispersive X-ray (EDX) spectrum were taken on a JEOL-2010 transmission electron microscope with an accelerating voltage of 200 kV. UV–vis spectra were recorded on a Solid Spec-3700 spectrophotometer at room temperature.

### 2.3. The photocatalytic measurements

The photocatalytic activity experiments on the obtained BiOBr samples for the decomposition of methyl orange in air were performed at room temperature. The degradation was carried out with a 500 W Xe lamp as the light source with a 420 nm cutoff filter to provide visible-light irradiation. BiOBr samples as catalysts (100 mg) were added to the aqueous methyl orange solutions (10 mg $L^{-1}$, 100 ml) and the suspensions were magnetically stirred in the dark for 30 min to reach the adsorption–desorption equilibrium between methyl orange and the catalysts. Then the suspensions were exposed to visible-light irradiation under magnetic stirring. At given time intervals, about 5 ml suspensions were sampled and centrifuged to remove the photocatalyst particles. Commercial $TiO_2$ powder (nanoparticles, surface area 50 $m^2\ g^{-1}$) was adopted as the reference, to compare the photocatalytic activity under the same experimental condition. UV–vis absorption spectra were recorded at different time intervals to monitor the reaction using a TU-1901 UV–vis spectrophotometer.

## 3. Results and discussion

### 3.1. BiOBr microflowers

#### 3.1.1. Structure and morphology characterization of BiOBr microflowers

Fig. 1 shows that the typical XRD pattern of the product prepared when 8 mmol of NaOH was added at 120 °C. All the diffraction peaks in the pattern can be indexed as the tetragonal phase of BiOBr (JCPDS Card no. 73-2061, space group $P4/nmm$). It is also worth noting that the (0 1 2) and (1 1 0) reflections show higher intensities than they would be, which indicates that the crystallites are abundant in (0 1 2) and (1 1 0) facets and thus their (0 1 2) and (1 1 0) planes tend to be preferentially oriented.

Fig. 2a shows a representative FESEM image at a low magnification of the product, which indicates that the main product consist of 3-D architectures with the size of about 10 μm. Closer inspection from a high magnification image (Fig. 2b) reveals that the microflowers are composed of nanoflakes. The surface of these flakes is smooth, and the thickness of the flakes is about 20 nm.

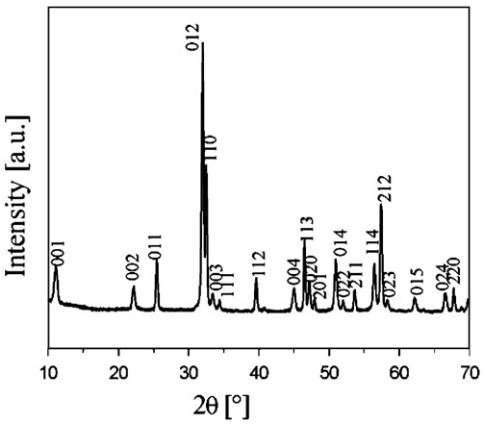


**Fig. 1.** X-ray power diffraction pattern of the product prepared with adding 8 mmol of NaOH at 120 °C.

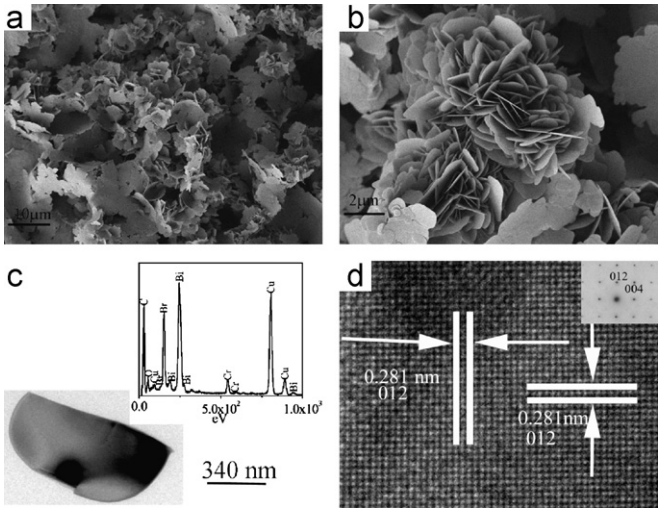


**Fig. 2.** Field-emission scanning electron microscopy images of the as-prepared BiOBr microflowers (a) low magnification, (b) high magnification, (c) transmission electron microscope image of a single BiOBr nanoflake (inset: EDX spectrum of a single nanoflake) and (d) high-resolution transmission electron microscopy image of a single nanoflake (inset: the corresponding SAED pattern).

Fig. 2c is a TEM image of an individual BiOBr nanoflake. The inset in Fig. 2d is the corresponding SAED pattern recorded from the nanoflake side. These pattern spots demonstrate the single crystal nature of BiOBr nanoflake. The bright spots shown in the SAED pattern could be indexed to (0 1 2) and (0 0 4) of tetragonal phase BiOBr. The ED pattern can be indexed to the diffraction pattern of [1 0 0] zone axis. An HRTEM image of an individual nanoflake shown in Fig. 2d presents the lattice spacings are about 0.281 nm, corresponding to the lattice spacings of the (0 1 2) planes for tetragonal structure BiOBr. The observed (0 1 2) and (0 0 4) lattices were projected along [1 0 0] axis, suggesting that the flake grow perpendicular to the [1 0 0] axis. These results are in well accordance with that of XRD pattern in Fig. 1. The inset in Fig. 2c is an EDX spectrum, only Bi, O, and Br peaks observed, indicating that the product is composed of Bi, O, and Br. Quantitative EDX analysis shows that the atom ratio of Bi/Br is 1:0.968, very close to 1:1.

#### 3.1.2. Possible formation mechanism of the BiOBr microflowers

To shed light on the formation mechanism of the 3D BiOBr microflowers, we studied the products at different reaction stages (10 min, 1, 3, 6 and 12 h) using FESEM technique. The FESEM images shown in Fig. 3 reveal the growth process of microflowers

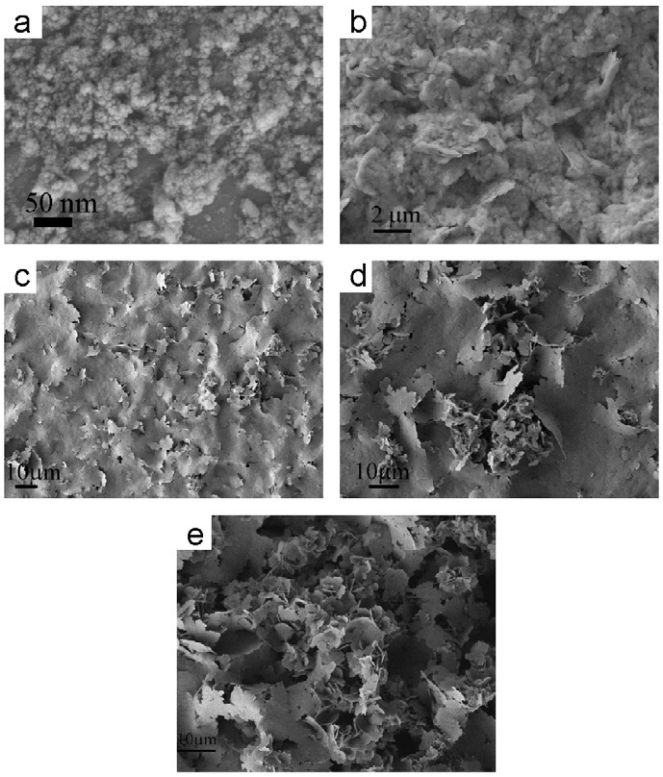


**Fig. 3.** FESEM images of BiOBr microflowers in different stages under 120 °C: (a) 10 min, (b) 1 h, (c) 3 h, (d) 6 h and (e) 12 h.

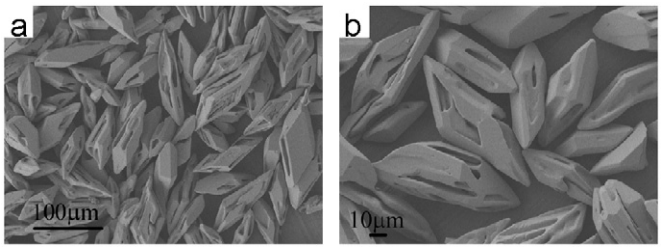


**Fig. 4.** Field-emission scanning electron microscopy images of the as-prepared $Bi_2O_3$ shuttles with concave surfaces (a) low magnification and (b) high magnification.

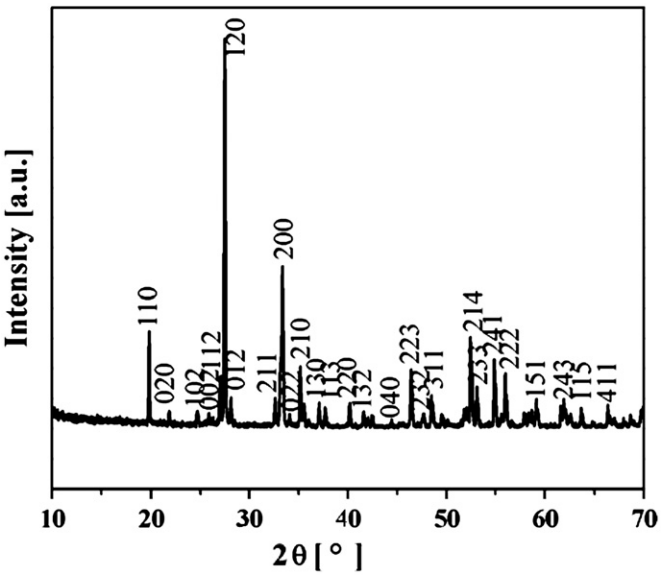


**Fig. 5.** X-ray power diffraction pattern of the product prepared by adding 28 mmol of NaOH at 120 °C.

from nanoparticles to microflowers. Fig. 3a shows that the product obtained at the beginning of 10 min is composed of many nanoparticles. After aging for 1 h the product is consisted of nanoparticles coexisting with some flakes (Fig. 3b). As shown in Fig. 3c, the product obtained at reaction time of 3 h is main 2D thin nanosheets. After reacting for 6 h, flower-like microstructures appear in the product (Fig. 3d). When the reaction time is prolonged to 12 h, almost all the product is 3D flower-like microstructure assembled by nanoflakes (Fig. 3e). The time-dependent experiments indicated that the Ostwald ripening process might be operative during the formation of BiOBr microflowers. From the above results, we believe that the growing process is consistent with the previous reports of a so-called two-stage growth process, which involves a fast nucleation of primary particles precursors followed by a slow aggregation and crystallization of the building blocks [20,21]. In our experiment, BiOBr nucleation resulted in the formation of primary nanoparticles at the beginning. These particles tended to grow anisotropically due to the intrinsic growth habit and aggregate into nanoflakes with the assistance of CTAB as the template through the Ostwald ripening process. Determined by special hindrance and some kinetic factors, the flakes could tend to curl and finally aggregated to 3D flower-like structures. Such a similar process has occurred in the preparation of $Fe_2O_3$, $CeO_2$, and $MnWO_4$ micro/nanoflowers [22–24].

### 3.2. $Bi_2O_3$ shuttles with concave surfaces

#### 3.2.1. Structure and morphology characterization of the $Bi_2O_3$ shuttles with concave surfaces

Keeping other experimental conditions unchanged and increasing the amount of NaOH to 28 mmol, a large amount of shuttles with the concave surfaces were formed in the product (Fig. 4a). Further detailed observation in Fig. 4b reveals that the shuttles are 100 μm in length and concave in every surface. All the diffraction peaks (Fig. 5) in the XRD of this product can be indexed as the monoclinic phase of $Bi_2O_3$ (JCPDS Card no. 76–1730, space group $P2_1/c$).

#### 3.2.2. Possible formation mechanism of the $Bi_2O_3$ shuttles with concave surfaces

To gain a better understanding of the growth process of the $Bi_2O_3$ shuttles with concave surfaces, the time course of the reaction is studied by means of FESEM images. Fig. 6 shows FESEM images of the as-prepared products obtained at different reaction periods. As can be seen from Fig. 6a, the products are flake-like particles at the initial 30 min. With the reaction time extended to 45 min, the flake-like particles begin to dissolve and several shuttles appear (Fig. 6b). After 50 min of growth, the flake-like particles and irregular shuttles coexist (Fig. 6c). With increasing the aging time to 1 h, most of flake-like particles are dissolved and a large amount of irregular shuttles are found (Fig. 6d). When the time is prolonged to 3 h, shuttles with small concave surfaces are formed (Fig. 6e). After aging for a longer period up to 12 h, as-obtained products are composed entirely of the shuttles with concave surfaces and the shuttles are 100 μm long (Fig. 6f).

On the basis of the above SEM observation and experimental process, a possible nucleation–dissolution–recrystallization growth mechanism is suggested to explain the formation of $Bi_2O_3$ shuttles with concave surfaces, which is often observed in hydrothermal synthesis of nanomaterials [25,26]. The formation mechanism of $Bi_2O_3$ shuttles with concave surfaces was deduced as follows. First,

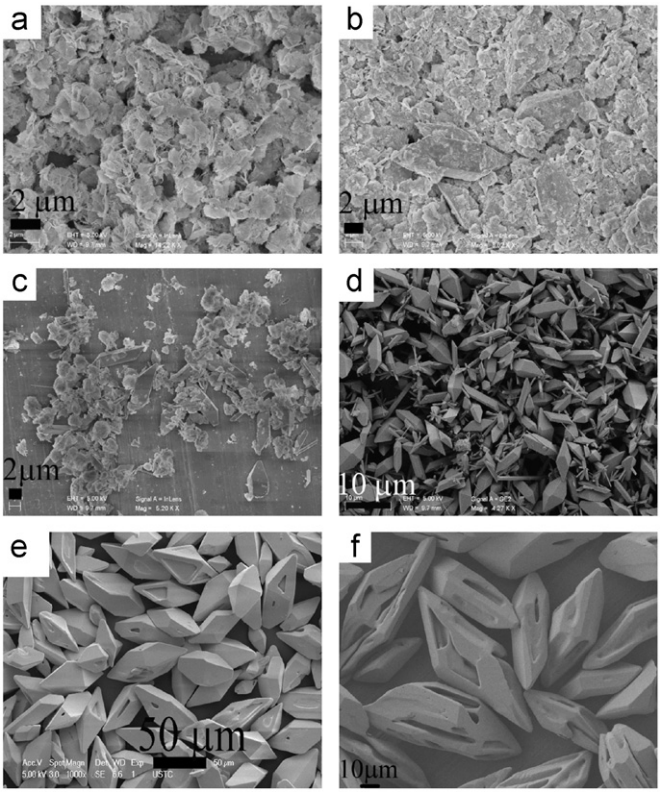


**Fig. 6.** FESEM images of the as-prepared $Bi_2O_3$ shuttles with concave surfaces in different time stages under 120 °C: (a) 30 min, (b) 45 min, (c) 50 min (d) 1 h, (e) 3 h and (f) 12 h.

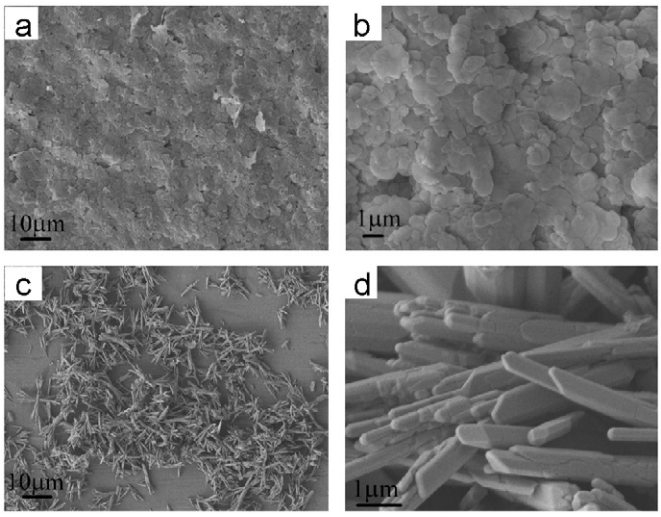


**Fig. 7.** FESEM images of the products obtained when the amount of NaOH is (a, b) 0 mmol and (c, d) 13 mmol.

**Table 1**
Amounts of NaOH employed in the synthesis and the compositions and morphologies of the resultant products.

| NaOH (mmol) | Compositions and morphologies of the resultant products |
|---|---|
| 0 | BiOBr nanoflakes |
| 8 | BiOBr microflowers |
| 13 | $Bi_2O_3$ rod clusters |
| 28 | $Bi_2O_3$ shuttles with the concave surfaces |

$Bi_2O_3$ slowly formed crystal nuclei from the solution. Due to intrinsic anisotropic growth habit of $Bi_2O_3$, these first-born crystal nuclei developed into flake-like particles. After heating, the flake-like particles started to dissolve into the solution and spontaneously nucleate. Then the crystallized particles grew aniscopically along the 3D direction, resulting in the formation of the shuttles. The shuttles grew until all the particles were consumed. The further detailed understanding of $Bi_2O_3$ shuttles with concave surfaces formation mechanism needs further investigation.

### 3.3. Influence factors

#### 3.3.1. Influence of CTAB on the BiOBr crystals

To investigate the influence of CTAB on the product, only irregular BiOBr nanoflakes were synthesized using NaBr as Br source under otherwise identical conditions. We changed the amount of CTAB with other parameters unchanged to investigate the influence of the formation of BiOBr microflowers. The product was not pure when adding 0.5 mmol of CTAB. Increasing the amount of CTAB to 2.5 mmol, the product was BiOBr nanoflakes with a small fraction of self-assembled lamellar structures. It is believed that the suitable concentration of $CTA^+OH^-$ provides appropriate condition for the growth of BiOBr microflowers.

#### 3.3.2. Influence factors of NaOH to the final products

In this reaction system, the amount of NaOH played a key role in controlling the composition and shapes of the final products. The reactions may proceed as follows:

$$Bi(NO_3)_3 + H_2O \rightarrow BiONO_3\downarrow + 2H^+ + 2NO_3^- \quad (1)$$

$$BiONO_3 + Br^- \rightarrow BiOBr\downarrow + NO_3^- \quad (2)$$

$$2BiONO_3 + 2OH^- \rightarrow Bi_2O_3\downarrow + H_2O + 2NO_3^- \quad (3)$$

First, the hydrolyzation of $Bi(NO_3)_3$ results in the formation of slightly soluble $BiONO_3$ under hydrothermal conditions [27,28]. After the employment of CTAB, the released $Br^-$ in the solution would exchange the nitrate ions located between the positively charged $BiO^+$ layers. After the anion exchange, BiOBr is produced in the solution. BiOBr crystals have been prepared hydrothermally in acidic aqueous solutions [1,29]. During our experiments, as the amount of NaOH is lower than 8 mmol added in the solution, BiOBr is the only product. When more NaOH is added, higher concentration of $OH^-$ ions react with $BiONO_3$. As the amount of NaOH reaches 13 mmol, $Bi_2O_3$ is the only product.

Fig. 7 shows the FESEM images of the samples prepared at different amounts of NaOH. As shown in Fig. 7a and b, the product is composed mainly of thin nanoflakes with size between 2 and 4 μm in the absence of NaOH. When 13 mmol of NaOH was added, uniform rod clusters were formed (Fig. 7c and d). The prism-like rods are about 10 μm in length and 0.5 μm in diameter. Table 1 summarizes the experimental conditions and morphologies of the products synthesized.

### 3.4. Optical absorption properties of BiOBr samples

The optical absorption properties of the as-obtained BiOBr samples have been investigated at room temperature by UV-visible spectroscopy (Fig. 7a). The BiOBr powders have intense absorption edges at 440 nm in the visible light region [14]. As a crystalline semiconductor, the optical absorption near the band edge follows the formula $\alpha h\nu = A(h\nu - E_g)^{n/2}$, where $\alpha$, $h$, $\nu$, $E_g$, and $A$ are the absorption coefficient, Planck constant, light frequency, band gap energy, and a constant, respectively [30]. Among them, $n$ depends on the characteristics of the transition in a semiconductor, i.e., direct transition ($n=1$) or indirect transition ($n=4$). For BiOBr, the value of $n$ is 4 for the indirect transition [31]. The

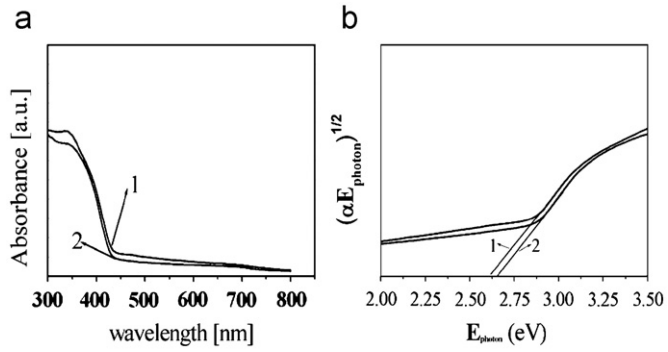


**Fig. 8.** (a) UV–vis diffuse reflection spectra of the as-obtained BiOBr microflowers (1) and BiOBr nanoflakes (2), (b) the plots of $(\alpha E_{photon})^{1/2}$ versus $\sim E_{photon}$.

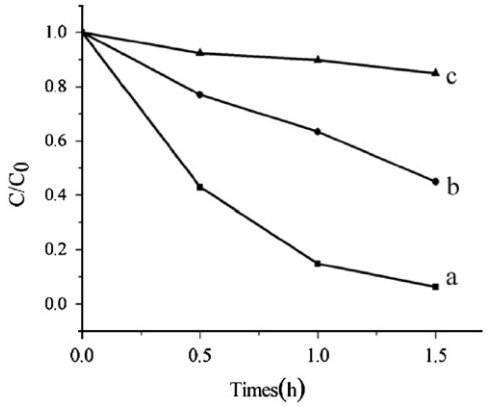


**Fig. 9.** Photodegradation efficiencies of MO mediated by the different photocatalysts (a) BiOBr microflowers; (b) BiOBr nanoflakes and (c) P25).

band gap energies ($E_g$ values) of BiOBr can be thus estimated from a plot of $(\alpha h\nu)^{1/2}$ versus photon energy ($h\nu$). The intercept of the tangent to the $x$-axis will give a good approximation of the band gap energies for the BiOBr powders. Plots of $(\alpha h\nu)^{1/2}$ versus photon energy ($h\nu$) of BiOBr powders are shown in Fig. 8b. The estimated band gap energies of the resulting samples were about 2.66 eV for BiOBr nanoflakes and 2.62 eV for BiOBr microflowers. The smaller band gap of BiOBr microflowers may be resulted from the quantum confinement effect of nanoflake structure. These results also indicate that all these BiOBr samples have suitable band gaps for photocatalytic decomposition of organic contaminants under visible light irradiation.

### 3.5. Photocatalytic activities of BiOBr samples

Methyl orange (MO) is selected as the model pollutant to evaluate the photocatalytic activity. Its characteristic absorption at about 464 nm has been used to monitor the photocatalytic degradation process [1,14]. MO is very stable and not decomposed even after long-term illumination with natural light in the absence of a photocatalyst. In addition, the concentration of MO almost does not reduce under dark conditions after the BiOBr powders are added into its aqueous solution and the solution reaches the adsorption–desorption equilibrium. Therefore, the presence of both a catalyst and illumination is necessary for efficient degradation of MO. Fig. 9 represents the variation of MO concentration ($C/C_0$) with irradiation time over different catalysts under Xe lamp irradiation. $C$ was the absorption of MO at the wavelength of 464 nm and $C_0$ was the absorption after the adsorption equilibrium on BiOBr before irradiation. A rapid

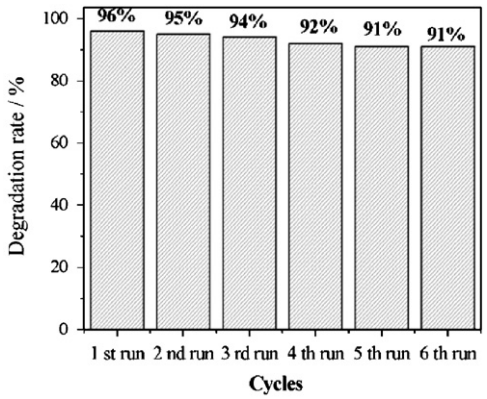


**Fig. 10.** Cycling runs of the BiOBr microflowers under visible-light irradiation.

decrease of MO absorption at the wavelength of 464 nm is observed. This indicates that the BiOBr microflowers exhibit excellent photocatalytic activity in the degradation of MO (Fig. 9a), which was up to 96% within 90 min. As a comparison, the photolysis of BiOBr nanoflakes (Fig. 9b) and $TiO_2$ (Degussa, P25) (Fig. 9c) were also performed under identical conditions. BiOBr nanoflakes degraded about 50% of MO and P25 only degraded about 10% of MO within 90 min. It was found that BiOBr microflowers were more active to degrade MO under the visible light irradiation than BiOBr nanoflakes.

By comparing the processes with P25, it is revealed that in the degradation of MO the photocatalytic process was the predominant process. The high photoactivity of BiOBr microflowers may be ascribed to two reasons: firstly, BiOBr nanostructure material itself have good photocatalyst activity [14,17]; secondly, the synthesized material microstructures also play an important role for high photoactivity. In general, the catalytic process is mainly related to the adsorption and desorption of reactant molecules on the surface of the catalysts. The BiOBr microflowers constructed from thinner nanoflakes held larger specific surface areas ($7.8\ m^2\ g^{-1}$) than that of BiOBr nanoflakes ($4.3\ m^2\ g^{-1}$). As a result, more coordination sites on the unsaturated surface are exposed to the MO solution, while the nanostructure of the microflowers allows more efficient transportation for the reactant molecules to move into the active sites [15], enhancing the efficiency of photocatalysis.

The photocatalytic activity experiments of $Bi_2O_3$ samples for the decomposition of methyl orange were also performed. However, the $Bi_2O_3$ samples showed weak photocatalytic activities, because the size of $Bi_2O_3$ shuttles with 100 μm in length and 50 μm in diameter at the middle of the shuttles are relatively large, which result in that the adsorption and desorption of MO on the surface of the $Bi_2O_3$ samples are difficult.

To test the stability and reusability of the BiOBr microflowers for the photocatalytic reaction, the catalyst was reused for photocatalytic reaction 6 times under the same conditions, and the result is shown in Fig. 10. The photocatalytic efficiency of the BiOBr microflowers decreases only 5% after six cycles. It indicates that the BiOBr microflowers prepared by this facile method are stable for the photocatalysis of pollutant molecules, which is important for its application.

## 4. Conclusion

In summary, in the reaction system of $Bi(NO_3)_3$–CTAB–NaOH, BiOBr and $Bi_2O_3$ with different shapes were hydrothermally synthesized by controlling the amount of NaOH added. As 8 mmol of NaOH was added, BiOBr microflowers assembled of nanoflakes

have been prepared. When the amount of NaOH was 28 mmol, $Bi_2O_3$ shuttles with concave surfaces were obtained. The amount of NaOH played a key role in controlling the compositions and morphologies of the final products. The photocatalytic activity of as-prepared BiOBr microflowers was evaluated by the degradation of methyl orange (MO) under visible-light irradiation, which was up to 96% within 90 min. The synthesized BiOBr microflowers are promising photocatalysts for degrading organic pollutants.

## Acknowledgment

We acknowledge the financial support from the 973 project of China (No. 2011CB935900).

## References

[1] W.D. Wang, F.Q. Huang, X.P. Lin, J.H. Yang, Catal. Commun. 9 (2008) 8–12.
[2] Z.H. Ai, W.K. Ho, S.C. Lee, L.Z. Zhang, Environ. Sci. Technol. 43 (2009) 4143–4150.
[3] G. Bandoli, D. Barecca, E. Brescacin, G.A. Rizzi, E. Tondello, Chem. Vap. Deposition 2 (1996) 238–242.
[4] M. Schuisky, A. Haarsta, Chem. Vap. Deposition 2 (1996) 235–238.
[5] M. Yashima, D. Ishimura, Chem. Phys. Lett. 378 (2003) 395–399.
[6] A. Feldman, W.S. Brower Jr., D. Horowitz, Appl. Phys. Lett. 16 (1970) 201–202.
[7] E.Y. Wang, K.A. Pandelisev, J. Appl. Phys. 52 (1981) 4818–4820.
[8] Z.N. Adamian, H.V. Abovian, V.M. Aroutiounian, Sens. Actuators, B 35–36 (1996) 241–243.
[9] A. Cabot, A. Marsal, J. Arbiol, J.R. Morante, Sens. Actuators, B 99 (2004) 74–89.
[10] A. Pan, A. Ghosh, J. Non-Cryst. Solids 271 (2000) 157–161.
[11] T.P. Gujar, V.R. Shinde, C.D. Lokhande, S.H. Han, J. Power Sources 161 (2006) 1479–1485.
[12] F.L. Zheng, G.R. Li, Y.N. Ou, Z.L. Wang, C.Y. Su, Y.X. Tong, Chem. Commun. 46 (2010) 5021–5023.
[13] Z.T. Deng, D. Chen, B. Peng, F.Q. Tang, Cryst. Growth Des. 8 (2008) 2995–3003.
[14] X. Zhang, Z.H. Ai, F.L. Jia, L.Z. Zhang, J. Phys. Chem. C 112 (2008) 747–753.
[15] J. Zhang, F.J. Shi, J. Lin, D.F. Chen, J.M. Gao, Z.X. Huang, X.X. Ding, C.C. Tang, Chem. Mater. 20 (2008) 2937–2941.
[16] L. Zhang, X.F. Cao, X.T. Chen, Z.L. Xue, J. Colloid Interf. Sci. 354 (2011) 630–636.
[17] M. Shang, W.Z. Wang, L.J. Zhang, J. Hazard. Mater. 167 (2009) 803–809.
[18] J.C. Yu, A.W. Xu, L.Z. Zhang, R.Q. Song, L. Wu, J. Phys. Chem. B 108 (2004) 64–70.
[19] F. Gao, Q. Lu, S. Komarneni, Chem. Commun. 4 (2005) 531–533.
[20] Y. Cheng, Y.S. Wang, Y.H. Zheng, Y. Qin, J. Phys. Chem. B 109 (2005) 11548–11551.
[21] R.L. Penn, J. Phys. Chem. B 108 (2004) 12707–12712.
[22] L.S. Zhong, J.S. Hu, H.P. Liang, A.M. Cao, W.G. Song, L.J. Wan, Adv. Mater. 18 (2006) 2426–2431.
[23] L.S. Zhong, J.S. Hu, A.M. Cao, Q. Liu, W.G. Song, L.J. Wan, Chem. Mater. 19 (2007) 1648–1655.
[24] Y. Xing, S.Y. Song, J. Feng, Y.Q. Lei, M.Y. Li, H.J. Zhang, Solid State Sci. 10 (2008) 1299–1304.
[25] G.C. Xi, Y.K. Liu, X.Q. Wang, X.Y. Liu, Y.Y. Peng, Y.T. Qian, Cryst. Growth. Des. 6 (2006) 2567–2570.
[26] J.H. Zhang, Q.H. Kong, J. Du, Y.T. Qian., J. Cryst. Growth 308 (2007) 159–165.
[27] A. Kudo, K. Omori, H. Kato, J. Am. Chem. Soc. 121 (1999) 11459–11467.
[28] Y. Yu, C. Jin, R. Wang, Q. Chen, L. Peng, J. Phys. Chem. B 109 (2005) 18772–18776.
[29] Z. Jiang, F. Yang, G.D. Yang, L. Kong, P.P. Edwards, J. Photochem. Photobiol., A 212 (2010) 8–13.
[30] M.A. Butler, J. Appl. Phys. 48 (1977) 1914–1920.
[31] K.L. Zhang, C.M. Liu, F.Q. Huang, C. Zheng, W.D. Wang, Appl. Catal. B 68 (2006) 125–129.